Physically-based auralization of railway rolling noise

Julien Maillard, Abbès Kacem, Nadine Martin, Baldrik Faure

Physically-based auralization of railway rolling noise

Julien MAILLARD[(1)], Abbes KACEM[(1)], Nadine MARTIN[(2)], Baldrik FAURE[(3)]

[(1)]Centre Scientifique et Technique du Bâtiment, Paris-Est University, 24 rue Joseph Fourier, 38400 Saint Martin d'Hères, France, julien.maillard@cstb.fr

[(2)]Univ. Grenoble Alpes, CNRS, Grenoble INP, GIPSA-lab, 38000 Grenoble, France

[(3)]Société Nationale des Chemins de Fer Français, 1/3 Avenue François Mitterrand, 93210 Saint-Denis, France

Abstract

Railway noise contributes significantly to noise pollution both outside and within cities. In recent years, prediction models have been developed to study exposure levels and evaluate abatement solutions. Going one step further, auralization may provide an effective mean for evaluating perceptually the impact of railway noise on the soundscape near existing or future infrastructures. This paper extends railway noise emission models to propose an auralization approach based on physical parameters. As a first step, the approach focuses on rolling noise radiated by the track and wheels, which represents the main noise source over a wide range of speed. The excitation of the wheel/rail system by surface roughness is modeled in the time domain based on the system mobilities. Next, rail emission is modeled as a set of discrete coherent monopoles, while the wheel contribution uses resonant filters based on its structural response. Finally, the contribution of track sleepers is included following the standard TWINS model. Validations of the approach compare auralized pass-by levels with measured data. Preliminary results from listening tests evaluating the realism of auralized pass-by noise samples are also presented.

Keywords: Auralization, Railway noise

1 INTRODUCTION

Railway infrastructures in urban areas represent a good solution to reduce the environmental impact of transportation. With comparatively low CO2 emissions, railway transportation represents however an important source of noise pollution. In this context, prediction tools are needed not only to evaluate and mitigate railway noise but also to inform and communicate with populations. Existing tools, such as the ACOUTRAIN software, manage to predict rolling stock emission levels based on experimental source characterization for the equipments and the TWINS model for rolling noise emission [1]. However, these models are limited to averaged levels per frequency bands. Consequently, they are not suited for realistic audio rendering and thus, perceptual evaluation. Also, these models in the frequency domain do not take into account impulsive sources such as the numerous rail joints present in urban railway networks, even though they contribute significantly to the perceived noise. Auralization [2] overcomes these limitations by synthesizing the time domain sound pressure signal perceived by a virtual listener in a simulated environment.

In this paper, we introduce a new approach for the auralization of rolling noise as a first step towards the auralization of railway noise as a whole. Previous studies have shown that rolling noise represents the main railway noise source at speed between 50 and 300 km/h [3]. The approach is based on an existing model for the simulation of rolling noise emission levels. This model, from which TWINS is also derived, has been shown to give reliable predictions [4] and is widely used in the community. It takes as inputs the spectrum of the combined roughness of the rolling surface of the wheels and rails, the track physical parameters and the train speed. It then calculates the interaction force between the rail and wheel [1]. The radiated sound levels are then predicted using a model of the vibro-acoustic response of the wheel, rail and sleeper structures. The auralization model in the present paper follows a similar approach, applied in the time domain, to propose appropriate audio signal processing for each one of the three rolling noise components.

Previous work on railway noise auralization started in 2005 within the SILENCE project which lead to the VAMPPASS software tool for the sound synthesis of a train pass-by [5]. In VAMPPASS, rolling noise is synthesized as a broad band signal shaped according to third octave spectra obtained from measurements or from the TWINS model. More recently, a time domain synthesis model was developed for rolling and impact railway noise [6]. The basis of the proposed model is the generation of the rail and wheel roughness as a broad band signal shaped according to the roughness spectrum. The resulting time signal is then fed to two filters modeling the vibro-acoustic behavior of the wheel and track with transfer functions based on the third octave band spectra of the CNOSSOS-EU railway noise emission model [7]. The modal behavior of the wheel/rail system is also included in order to improve the realism of the synthesis. Even though it has not been formally evaluated, the realism of this method appears superior compared to previous work.

The approach presented below introduces an improved auralization model to obtain realistic sound rendering of rolling noise for any wheel/rail system, based on its physical parameters. Unlike previous work, the rail contribution is modeled as an extended multi-source distribution in order to preserve the rail radiation characteristics. In Section 2, the model is described starting with the rail and wheel response, the wheel/rail excitation force and signal processing of the auralization system. In Section 3, measured and auralized pass-by signals are compared in terms of sound pressure levels and perceived realism.

2   APPROACH

Railway rolling noise results from rail, wheels and sleepers vibrations [1]. The analysis of each component shows that their acoustic contribution dominates the overall response in distinct frequency regions. Therefore, all three sources must be accounted for in the proposed auralization model. Figure 1 shows the overall schematic of this model for one wheel/rail contact. In this figure, the blue-colored blocks represent signal processing modules.
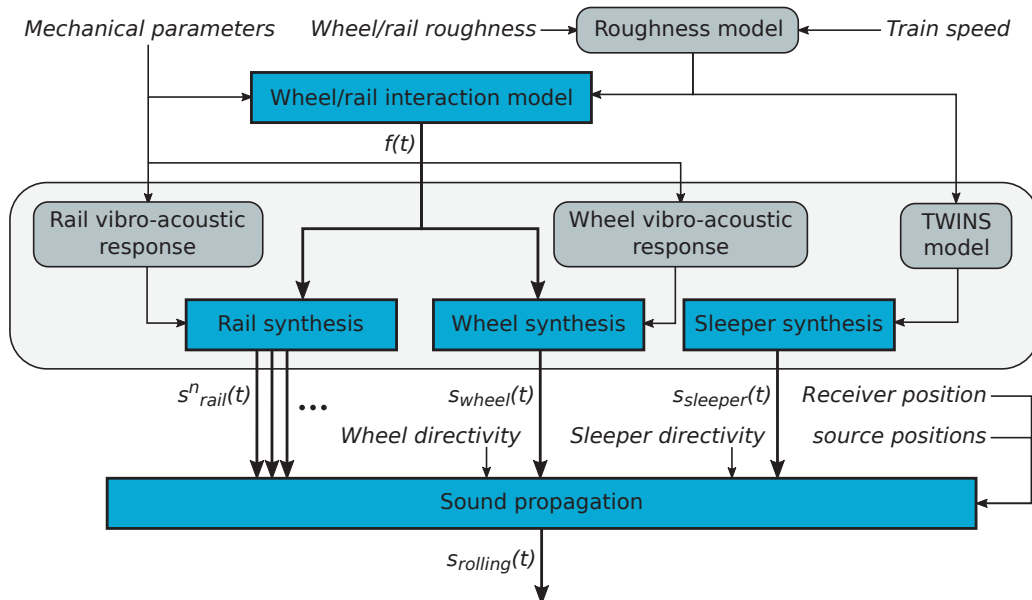

Figure 1. Schematic of the auralization model for one wheel/rail contact.

Signal paths in the time domain are represented as thick line arrows. The grey-colored blocks correspond to models in the frequency domain. The model inputs consist of the mechanical parameters of the wheel/rail system, the combined roughness of the wheel and rail contact surfaces and the train speed. Note that train

speed may vary in time. First, the roughness input spectrum is converted to a frequency spectrum based on train speed. The wheel/rail interaction model then constructs the time domain signal of the vertical interaction force, $f(t)$, between the rail and wheel. Next, this signal is fed to two filter modules representing the acoustic response, to a unit excitation force, of the rail and wheel structure, respectively. The rail synthesis module generates N acoustic emission signals, $s_{rail}^n(t)$, $n = 1, \ldots, N$, associated with the N monopole sources of the rail radiation model. The wheel synthesis module generates a single emission signal, $s_{wheel}(t)$. The third synthesis module generates the contribution of the track sleeper, $s_{sleeper}(t)$. This contribution is obtained from the TWINS model using the wheel/rail combined roughness as input. Finally, the sound propagation module applies source to receiver propagation effects to each emission signals, including the frequency dependent directivity of the wheel and sleeper emission models. The overall radiated sound pressure signal, $s_{rolling}(t)$, is obtained as the sum of all contributions. In the following sections, we further discuss each step of the auralization process.

2.1 Vibro-acoustics response of the rail

The rail roughness excitation is mainly in the vertical direction. It produces vertical flexural waves propagating on each side of the wheel/rail contact point. These waves are the main source of rail noise. Following previous work [1, 8], the vertical rail response is modeled as an infinite beam continuously supported by a mass between two spring-damper layers, representing the rail pads, sleepers, and ballast. Assuming a $e^{i\omega t}$ time dependence with t, the time and ω, the angular frequency, the rail vertical mobility is expressed as

$$Y_r(x, \omega) = i\omega \left[A_c(\omega) e^{-\gamma_c(\omega)|x - x_e|} + iA_p(\omega) e^{-\gamma_p(\omega)|x - x_e|} \right]. \tag{1}$$

where x is the horizontal axis along the rail rolling surface, x_e, the position of the excitation, $A_c(\omega)$, $\gamma_c(\omega)$, and $A_p(\omega)$, $\gamma_p(\omega)$, the amplitude and propagation constant of the near-field and propagating waves, respectively. The propagating structural wave speed is as $c_{rail}(\omega) = \omega/\lambda_{rail}(\omega)$ with $\lambda_{rail}(\omega) = \Im[\gamma_p(\omega)]$, the wave-number and $\Im[.]$, the imaginary part operator. The structural decay rate of the rail vertical flexural wave in [dB/m] is defined as $\Delta_s(\omega) = 20\Re[\gamma_p(\omega)]\log_{10}(e)$ where $\Re[.]$ is the real part operator. As an example, the decay rate is plotted versus frequency in Figure 2 for two sets of track parameters listed in Table 1 corresponding to a concrete sleeper track with low and medium stiffness supports, respectively. Parameters derived from the measured decay rate on the track used for the pass-by recordings is also included. This third track (last column of Table 1) has wood sleepers with stiff supports. As seen in Figure 2, the decay rate is small (about
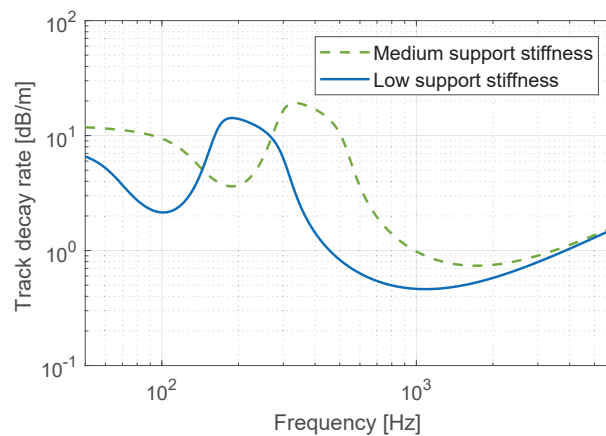

Figure 2. Rail vertical flexural wave decay rate calculated for the track parameters of Table 1 (concrete sleepers with "medium" and "low" stiffness supports).

1 dB/m) at high frequencies: vibrations propagate far away from the excitation point and a spatially extended

Table 1. Rail and track properties used in the simulations.

Rail		Track	medium	low	high
Bending stiffness [MN m^2]	6.42	Pad stiffness [MN/m]	300	100	210
Rail loss factor	0.02	Pad loss factor	0.2	0.2	1.35
Shear coefficient	0.4	Sleeper mass [kg]	240	240	72.8
Density [kg/m^3]	8000	Sleeper spacing [m]	0.6	0.6	0.6
Mass per length [kg/m]	60	Ballast stiffness [MN/m]	100	25	25
Poisson's ratio	0.3	Ballast loss factor	0.5	0.5	2

source model is required to represent the rail acoustic emission. As previously proposed, the model uses a line of coherent monopoles [1] equally spaced along the rail longitudinal axis. The spacing between monopoles is frequency dependent and chosen as a fraction, e.g., 1/5, of the smallest value between the acoustic and structural wavelengths. The number of monopoles is chosen such that the structural response is attenuated by a given factor, e.g., 60 dB, past the distribution end points. The complex volume velocity amplitude of monopole n, $Q(x_n, \omega)$ is proportional to the rail mobility $Y_r(x_n, \omega)$ at x_n,

$$Q(x_n, \omega) = Q_0(\omega) Y_r(x_n, \omega), \tag{2}$$

where the constant $Q_0(\omega)$ can be derived analytically [1].

2.2 Vibro-acoustics response of the wheel

Due to its finite geometry and material properties, the wheel response can be expressed using modal super-position. The vertical and axial wheel mobility at location $\mathbf{s}$ on the web surface, $Y_w(\mathbf{s}, \omega)$, due to a vertical excitation is approximated as the sum of the response of the first N modes,

$$Y_w(\mathbf{s}, \omega) = \sum_{n=1}^{N} \frac{A_n(\mathbf{s})}{\omega_n^2 - \omega^2 + 2i\zeta_n \omega \omega_n}, \tag{3}$$

where the modal parameters A_n, ω_n and ζ_n are the amplitude, resonant frequency and damping factor, respectively, of mode n. In this work, the above parameters were characterized during previous experimental measurements on a fixed monobloc wheel [9]. They could also be estimated from the finite element method.

The wheel radiated pressure can then be evaluated in the far field using the Rayleigh approximation applied to the axial velocity distribution given by Eq. (3). Integrating the far-field pressure over a hemisphere enclosing the wheel and using the orthogonality property of the structural modes, the wheel emitted sound power is then written as

$$W(\omega) = \frac{\rho \omega^2}{4\pi c} \sum_{n=1}^{N} \frac{|A_n|^2}{\left|\omega_n^2 - \omega^2 + 2i\zeta_n \omega \omega_n\right|^2}. \tag{4}$$

where ρ is the air density and c, the sound speed. The wheel is now replaced by an equivalent point-source with sound power, $W(\omega)$, and directivity function, $D(\theta, \phi, \omega)$, where θ and ϕ are the azimuth and elevation angles, respectively.

2.3 Wheel/rail interaction force signal

The structural and acoustic response of the wheel/rail system for a vertical unit excitation being established, this section now presents the time model of the interaction force. It is based on the vertical wheel/rail interaction model introduced by Thompson [1]. The force amplitude in the vertical direction is expressed as $F(\omega) = R(\omega)F^{unit}(\omega)$ with $R(\omega)$, the combined roughness amplitude, and $F^{unit}(\omega)$, a unit roughness point force,

$$F^{unit}(\omega) = \frac{i\omega}{Y_r(x_e, \omega) + Y_w(x_e, \omega) + Y_c(\omega)}, \tag{5}$$

where $Y_r(x_e, \omega)$, $Y_w(x_e, \omega)$ and $Y_c(\omega)$ are the vertical mobilities, at the point of contact, of the rail, the wheel and the contact spring, respectively. The contact spring is used to model the wheel/rail connection. Its mobility is defined as $Y_c(\omega) = i\omega/K_H$ where K_H is the linearized contact stiffness, with a standard value of 950 MN/m. Note that the contact force spectrum, $F^{unit}(\omega)$ exhibits peaks due to the wheel mobility resonance frequencies.

The excitation model of Eq. (5) is now converted in the time domain to construct the wheel/rail contact force signal $f(t)$, as the convolution of a continuous roughness signal $r(t)$ with the impulse response of the unit roughness contact force $f^{unit}(t)$,

$$f(t) = r(t) * f^{unit}(t), \tag{6}$$

where $*$ denotes the convolution product. The unit roughness contact force $f^{unit}(t)$ is obtained as the inverse Fourier transform of $F^{unit}(\omega)$. Similar to the approach proposed by Pieren [6], the roughness signal $r(t)$ is generated as a filtered white noise with third octave band spectral shaping:

$$r(t) = \sum_{u=1}^{U} R(\omega_u) . \xi_u(t), \tag{7}$$

where $\xi_u(t)$ denotes the normalized signal in band u and U is the number of frequency bands. The combined roughness RMS amplitude spectrum, $R(\omega_u)$, is obtained as the sum of the wheel and rail roughness expressed as a function of wavelength. A contact filter is then applied to model the effect of the extended contact area between the wheel and rail [10]. Finally, the roughness is expressed as a function of frequency ω_u using the relation $\omega_u = 2\pi V/\lambda_u$ where V is the wheel speed in m/s and λ_u is the roughness wavelength in m.

2.4 Auralization

Recalling Figure 1, the auralization process begins by generating the contact force signal, $f(t)$, as described in Section 2.3 above. For each frequency band u, the rail equivalent monopole sources are distributed on each side of the contact point. The number N_{ω_u} and locations of the discrete equivalent sources, x_n, $n = 1..N_{\omega_u}$, are defined such as to satisfy the constraints of source separation and spatial extent at ω_u, outlined in Section 2.1. The rail n^{th} monopole source signal in frequency band u is obtained as

$$s_{n,u}(t) = \alpha_{n,u}(t) \ f_u(t - \tau_{n,u}(t)) \tag{8}$$

where the force signal component in frequency band u, $f_u(t)$, is obtained as $f_u(t) = r_u(t) * f^{unit}(t)$ with $r_u(t) = R(\omega_u) . \xi_u(t)$, the roughness signal in band u and $f^{unit}(t)$, the excitation force per unit roughness. The amplitude $\alpha_{n,u}(t)$ represents the sound pressure amplitude radiated by monopole n at frequency ω_u for a unit force excitation at the receiver position. It is function of the monopole volume velocity amplitude given in Eq. 2 and the source to receiver geometrical spreading factor and possibly additional propagation effects. The propagation delay, $\tau_{n,u}$, for the same source is calculated as

$$\tau_{n,u}(t) = \frac{r_n(t)}{c} + \frac{|x_n - x_e|}{c_{rail}(\omega_u)}, \tag{9}$$

where $r_n(t)$ is the source-receiver distance and c_{rail}, the frequency dependent speed of the flexural waves in the rail. The above delay includes both sound propagation in air and the phase offset between monopoles induced by the finite structural wave speed. Note that $\alpha_{n,u}(t)$ and $\tau_{n,u}(t)$ are time dependent due to wheel motion. The rail total sound pressure signal is then obtained by summing signals $s_{n,u}(t)$ over all bands and monopoles.

To retain the modal behavior of the railway wheel in the emission synthesis, the wheel source signal generation uses a series of damped harmonic resonators with resonant frequency, damping factor and amplitude derived from the radiated pressure at distance 1 m from the wheel equivalent source, with power given by Eq. (4). The sound pressure source signal emitted by the wheel at 1 m is then obtained as

$$s_{wheel,1\text{m}}(t) = \sum_{n=1}^{N} f(t) * h_n(t), \tag{10}$$

with N, the number of resonance modes and $h_n(t)$, the impulse response of resonator n.

The sleeper contribution is modeled as a single point source, located at the wheel/rail contact point. The equivalent source levels are based on the TWINS model which calculates sleeper emission levels in third octave bands as a function of roughness amplitudes [1]. The sleeper signal is constructed using a band filtered white noise as for the excitation force signal.

The wheel and sleeper equivalent source pressure signals at 1 m are then propagated to the receiver position including directivity, propagation delay and attenuation effects.

3 RESULTS

The proposed approach is now applied to construct pass-by sound samples and compare them to recorded signals of a real train pass-by. Measurements of a Bombardier AGC passenger train composed of 4 wagons and 5 bogies, with 2 wheels per bogie, were carried out on a dedicated track. Train speed is set to 80 km/h for which pass-by noise is dominated by the rolling noise contribution. Measurements include two distances from the track, 7.5 m and 25 m. The track decay rate and surface roughness were both measured. Wheel roughness was assumed to be close to previously measured data on a similar wheel. It should be pointed out that measured decay rate exhibits unusually high values above 2000 Hz. The track parameters derived from this measured decay rate, referred to as "high" in Table 1, result in strong fluctuations of each wheel pass-by levels, the rail behaving as a localized point source above 2000 Hz. However, the same level fluctuations are not present on the recorded pass-by samples. It was thus decided to test another set of track parameters, referred to as "low" in Table 1, with values matching standard decay rate measurements found in the literature. All simulated pass-by samples use $U = 22$ third octave bands between 50 and 6300 Hz, thus covering the
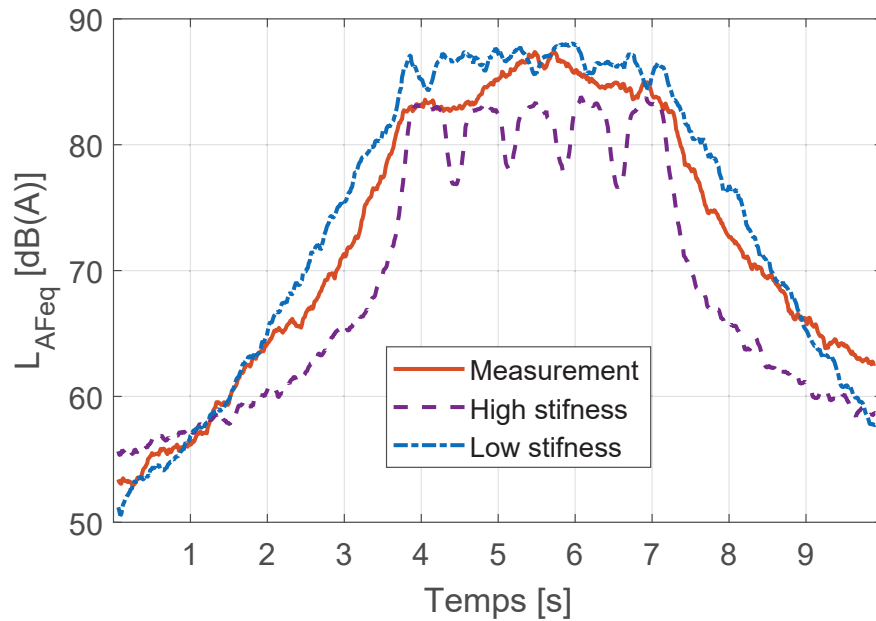

Figure 3. A-weighted pass-by sound pressure level at 80 km/h: measured (red solid line), $L_{Aeq} = 80.4$ dB(A); auralized, high stiffness (purple dashed line), $L_{Aeq} = 77.9$ dB(A); auralized, low stiffness (dashed-dotted blue line), $L_{Aeq} = 82.7$ dB(A).

main frequency content of rolling noise. The wheel directivity follows the CNOSSOS-EU simplified emission

model [7], and the sleeper contribution is assumed omni-directional [1]. The test samples are generated for several model configurations. Wheel damping is known to increase under rolling conditions compared to values measured on fixed wheels. Simulated samples thus include a 10 time and a 20 time damping factor. Three rail equivalent source distributions are also included: a single-source configuration with the CNOSSOS-EU rail directivity, and two multi-source configurations with 5 and 2 monopoles per wavelength and distribution lengths associated with a 60 dB and a 5 dB attenuation, respectively.

Figure 3 compares the A-weighted sound pressure level, L_{AFeq}, using a 125 ms (fast) averaging window, of the simulated and measured sound samples during the train pass-by at 7.5 m. The simulated samples both use a rail source distribution with 5 monopole per wavelength and a 60 dB attenuation length and a 20 time damping factor. The influence of rail support stiffness on the radiated sound field can be clearly seen on the curves. As explained above, the high support stiffness generates strong level fluctuations which are not present on the measured levels. The low support stiffness better match the measured levels. Further improvements could be achieved with better track parameter identification.

Next, listening tests were carried out to assess the perceived realism of the auralized pass-by noise. Twenty participants (17 male, 3 female), aged from 21 to 53 years old are asked to judge the realism of a set of simulated samples in comparison with the recorded pass-by sample used as the reference. The perceived realism obtained for the first 7.5 m distance is presented in Figure 4. Results show that the single-source rail emission
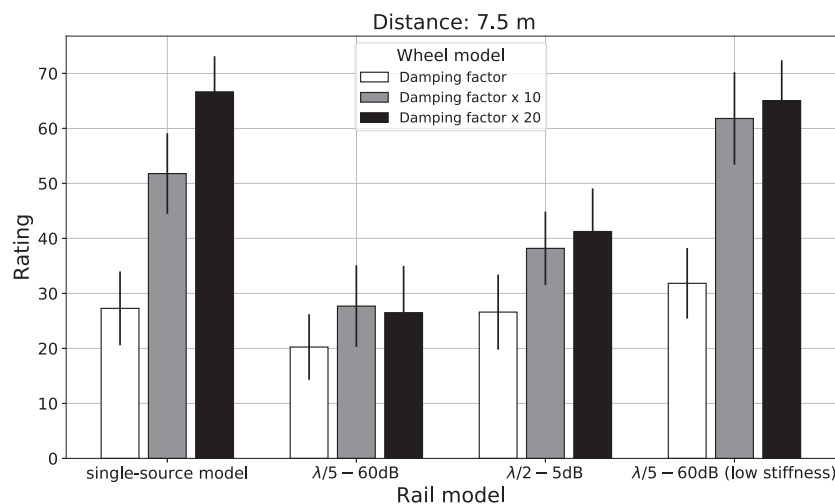

Figure 4. Listening test ratings of realism. Ratings ranged from 0 (very poor realism) to 100 (very high realism). Results are averaged across participants and repetitions. Vertical bars represent the 95% confidence interval of the mean value.

model is better perceived than the multi-source version based on the same track parameters. This is explained by the strong level fluctuations resulting from the high support stiffness which do not occur on the measured sample. The single source model does not contain these fluctuations and therefore sounds closer to the measured case. Using the low stiffness track parameters yields improved simulated samples in terms of perceived realism. In this case, realism is similar to the single-source distribution. Results also show that higher wheel damping improve realism compared to damping values measured on a fixed wheel which is consistent with previous results showing damping increases under rolling conditions.

4 CONCLUSIONS

This paper introduces a new auralization model for railway rolling noise based on the physical parameters of the wheel and track. The approach models the excitation of the wheel/rail system induced by surface roughness in the time domain, based on the rail and wheel mobility functions. Rail and wheel noise is then obtained by filtering the excitation signal through the modeled vibro-acoustic response of each structure. The rail emission uses a line of coherent monopoles to preserve the spatial characteristics of the radiated sound field. The wheel response which is dominated by its structural modes is modeled as a set of resonant filters. Finally, track sleeper noise is included in the synthesis following the TWINS model.

The proposed model is evaluated quantitatively and perceptually by comparing auralized pass-by noise with a real train pass-by recording at 7.5 m from the track. Results show that A-weighted short-time averaged sound pressure levels are predicted within 2 dB, provided the track parameters are well estimated. Preliminary analysis of the listening tests show that the model configuration such as support stiffness, rail structural damping and multi-source distribution, has an influence of the perceived realism. Overall, when properly configured, the proposed technique yields very realistic sounds with perceived realism between 6.5 and 7 on a 0 to 10 scale.

REFERENCES

[1] DJ Thompson. *Railway noise and vibration: mechanisms, modelling and means of control*. Elsevier, 2009.

[2] Michael Vorländer. *Auralization: fundamentals of acoustics, modelling, simulation, algorithms and acoustic virtual reality*. Springer Science, 2008.

[3] Cyril Mellet, Fabien Létourneaux, Frank Poisson, and Corinne Talotte. High speed train noise emission: Latest investigation of the aerodynamic/rolling noise contribution. *Journal of sound and vibration*, 293(3-5):535–546, 2006.

[4] CJC Jones and DJ Thompson. Extended validation of a theoretical model for railway rolling noise using novel wheel and track designs. *Journal of Sound and Vibration*, 267(3):509–522, 2003.

[5] Estelle Bongini, Stephane Molla, Cédric Herviou, Dominique Habault, and Franck Poisson. Prediction and audio synthesis of vehicle pass-by noise. *Acoustics08 Paris*, 2008.

[6] Reto Pieren, Kurt Heutschi, Jean Marc Wunderli, Mirjam Snellen, and Dick G Simons. Auralization of railway noise: Emission synthesis of rolling and impact noise. *Applied Acoustics*, 127:34–45, 2017.

[7] CNOSSOS-EU. European commission, commission directive (eu) 2015/996 of 19 may 2015 establishing common noise assessment methods according to directive 2002/49/ec of the european parliament and of the council. *Official Journal of the European Union 58*, 2015.

[8] Baldrik Faure, Olivier Chiello, Marie-Agnès Pallas, and Christine Serviere. Characterisation of the acoustic field radiated by a rail with a microphone array: The sweam method. *Journal of Sound and Vibration*, 346:165–190, 2015.

[9] Pierre-Emile Chartrain. *Lecture acoustique de la voie ferrée*. PhD thesis, Aix Marseille Université, 2013.

[10] Paul J Remington. Wheel/rail rolling noise, ii: validation of the theory. *The Journal of the Acoustical Society of America*, 81(6):1824–1832, 1987.